Article

An MHD Fluid Flow over a Porous Stretching/Shrinking Sheet with Slips and Mass Transpiration

A. B. Vishalakshi [1], U. S. Mahabaleshwar [1,*] and Ioannis E. Sarris [2]

1 Department of Mathematics, Davangere University, Shivagangothri, Davangere 577 007, India; vishalavishu691@gmail.com

2 Department of Mechanical Engineering, University of West Attica, 250 Thivon and P. Ralli Str., 12244 Athens, Greece; ioannisarris@gmail.com

* Correspondence: u.s.m@davangereuniversity.ac.in

Abstract: In the present paper, an MHD three-dimensional non-Newtonian fluid flow over a porous stretching/shrinking sheet in the presence of mass transpiration and thermal radiation is examined. This problem mainly focusses on an analytical solution; graphene water is immersed in the flow of a fluid to enhance the thermal efficiency. The given non-linear PDEs are mapped into ODEs via suitable transformations, then the solution is obtained in terms of incomplete gamma function. The momentum equation is analyzed, and to derive the mass transpiration analytically, this mass transpiration is used in the heat transfer analysis and to find the analytical results with a Biot number. Physical significance parameters, including volume fraction, skin friction, mass transpiration, and thermal radiation, can be analyzed with the help of graphical representations. We indicate the unique solution at stretching sheet and multiple solution at shrinking sheet. The physical scenario can be understood with the help of different physical parameters, namely a Biot number, magnetic parameter, inverse Darcy number, Prandtl number, and thermal radiation; these physical parameters control the analytical results. Graphene nanoparticles are used to analyze the present study, and the value of the Prandtl number is fixed to 6.2. The graphical representations help to discuss the results of the present work. This problem is used in many industrial applications such as Polymer extrusion, paper production, metal cooling, glass blowing, etc. At the end of this work, we found that the velocity and temperature profile increases with the increasing values of the viscoelastic parameter and solid volume fraction; additionally, efficiency is increased for higher values of thermal radiation.

Keywords: porous sheet; MHD; three-dimensional; thermal efficiency; exact solution; nanofluid

1. Introduction

Transport is one of the main motivations for conducting an experiment on stretching sheet problems, the main reason this problem is widely utilized in the engineering and industrial processes viz., extrusion of sheet, metal thinning, exchange of heat between, etc. Sakiadis [1,2] was the first researcher to investigate the stretching sheet problem. Later, Crane [3] elaborated this problem with flow past a stretching sheet. Motivated by Crane's work, many researchers conducted experiments on stretching sheet problems by observing their huge applications. Turkyilmazoglu [4] investigated the impact of MHD on thermal slip flow due to stretching sheet. Mahabaleshwar et al. [5–7] conducted experiments with magneto hydrodynamics in the presence of different physical parameters such as mass transpiration, thermal radiation, and Dufour and Soret mechanisms. Later, these investigations were carried out with porous sheet; these porous particles play a major role in stretching sheet problems as these porous materials help to enrich the rate of heat transfer from stretching/shrinking surfaces and have numerous industrial applications. Therefore, many researchers show interest in investigating porous media. Elboshbeshy and Bazid [8,9] investigated variable viscosity fluid flow with a porous medium and internal

heat generation. Further, this work was extended by Cortell [10]; he included power law temperature distribution. Mahabaleshwar et al. [11–14] demonstrated many porous stretching sheet problems with different flow fluids and a variety of boundary conditions. Rasool et al. [15] worked on second grade nanofluid flow with the Darcy–Forchheimer medium in the presence of thermal radiation and viscous dissipation (see further recent works on nanofluids in [16–18]).

Apart from these discoveries, some experiments take place with nanofluids, as these nanofluids offer a better thermal efficiency than base fluids. Rahman et al. [19] examined the nanofluid flow with porous exponential on the basis of Buongiorno's method. Mahabaleshwar et al. [20] and Benos et al. [21] examined the problem statement analytically in the presence of nanofluid. Shafiq et al. [22] investigated thermally enhanced Darcy–Forchheimer Casson-water/Glycerin rotating nanofluids by using the effect of uniform magnetic field. Rasool et al. [23] worked on MHD nanofluid flow on the basis of numerical scrutinization of Darcy–Forchheimer relation bound by nonlinear stretching surface with heat and mass transfer. Rasool and Shafiq [24] explained the Darcy medium with thermally enhanced chemically reactive Powell–Eyring nanofluid flow over a non-linearly stretching surface affected by a transverse magnetic field with convective boundary conditions. Afridi et al. [25] studied the 3-D dissipative flow with hybrid nanofluid; in this work, thermophysical models were used to investigate the entropy generation. Dianchen Lu et al. [26] examined the entropy generation by considering dissipative nanofluid flow by using the effect of magnetic dissipation and transpiration. Graphene is one of the most useful nanomaterials as it has an extraordinary blend of superb properties, better heat and electrical conduction, and optical transparency compared to other materials. Additionally, graphene is the thinnest as well as the strongest material. Some recent works on graphene are given in [27–29].

The present work is motivated by the work of Turkyilmazoglu [30], explaining the analytical solution of 3-D flow of a fluid with magneto hydrodynamics by using various physical parameters. Motivated by the abovementioned articles, the present work explains the three-dimensional flow of a non-Newtonian fluid due to porous stretching/shrinking sheet. Magneto hydrodynamics and graphene water nanoparticles are also immersed in the flow of fluid to achieve better thermal efficiency. The given PDEs are converted into ODEs by using similarity variables. Incomplete gamma function is obtained at the end of the solution. By using various physical parameters, the problem is verified exactly, and the skin friction coefficient is examined. The novelty of the present work is to examine the problem analytically and to find the domain in terms of mass transpiration; this is used in the heat transfer to analyze the heat equation. The work is used in many industrial and engineering applications, viz., power engines, advanced nuclear systems, automobiles, biological sensors, drug delivery, and entropy generation [31].

Problem Statement

An MHD graphene water nanofluid flow through a porous medium with mass transpiration and thermal radiation is considered. The physical diagram of the given problem is represented in Figure 1. Three-dimensional flow is subjected to wall temperature T_w in a porous medium and a far-field temperature T_∞. The porous medium is filled with graphene water nanoparticles. The quantities of nanofluid are indicated in Table 1. The equations of the fluid flow can be written in the form (see Mahabaleshwar et al. [32], Siddheshwar et al. [33] and Riaz et al. [34]).

$$\frac{\partial u}{\partial x} + \frac{\partial v}{\partial y} + \frac{\partial w}{\partial z} = 0 \tag{1}$$

$$
\begin{aligned}
u\frac{\partial u}{\partial x} + v\frac{\partial u}{\partial y} \quad &+ w\frac{\partial u}{\partial z} = \nu_{nf}\frac{\partial^2 u}{\partial z^2} + \gamma_0 u - \left(\frac{\mu_{nf}}{K\rho_{nf}} + \frac{\sigma_{nf} B_0{}^2}{\rho_{nf}}\right) u \\
&k\left\{ u\frac{\partial^3 u}{\partial x \partial z^2} + w\frac{\partial^3 u}{\partial z^3} - \left(\frac{\partial u}{\partial x}\frac{\partial^2 u}{\partial z^2} + \frac{\partial u}{\partial z}\frac{\partial^2 w}{\partial z^2} + 2\frac{\partial u}{\partial z}\frac{\partial^2 u}{\partial x \partial z} + 2\frac{\partial w}{\partial z}\frac{\partial^2 u}{\partial z^2}\right) \right\}
\end{aligned}
\tag{2}
$$

$$u\frac{\partial v}{\partial x} + v\frac{\partial v}{\partial y} + w\frac{\partial v}{\partial z} = \nu_{nf}\frac{\partial^2 v}{\partial z^2} + \gamma_0 v - \left(\frac{\mu_{nf}}{K\rho_{nf}} + \frac{\sigma_{nf}B_0^2}{\rho_{nf}}\right)v$$
$$k\left\{v\frac{\partial^3 v}{\partial y\partial z^2} + w\frac{\partial^3 v}{\partial z^3} - \left(\frac{\partial v}{\partial y}\frac{\partial^2 v}{\partial z^2} + \frac{\partial v}{\partial z}\frac{\partial^2 w}{\partial z^2} + 2\frac{\partial v}{\partial z}\frac{\partial^2 v}{\partial y\partial z} + 2\frac{\partial w}{\partial z}\frac{\partial^2 v}{\partial z^2}\right)\right\} \tag{3}$$

$$u\frac{\partial T}{\partial x} + v\frac{\partial T}{\partial y} + w\frac{\partial T}{\partial z} = \frac{\kappa_{nf}}{(\rho C_P)_{nf}}\frac{\partial^2 T}{\partial y^2} - \frac{1}{(\rho C_P)_{nf}}\frac{\partial q_r}{\partial y} \tag{4}$$

Subjected to appropriate boundary conditions are:

$$\left.\begin{array}{l} u = dax + l\frac{\partial u}{\partial z}, \ v = by + l\frac{\partial v}{\partial z}, \ w = w_0, \ -\kappa\frac{\partial T}{\partial z} = h(T_w - T), \ \text{at} \ z = 0 \\ u \to 0, \ \frac{\partial u}{\partial z} \to 0, \ v \to 0, \ \frac{\partial v}{\partial z} \to 0, \ T \to T_\infty \qquad\qquad\qquad \text{as} \ z \to \infty \end{array}\right\} \tag{5}$$
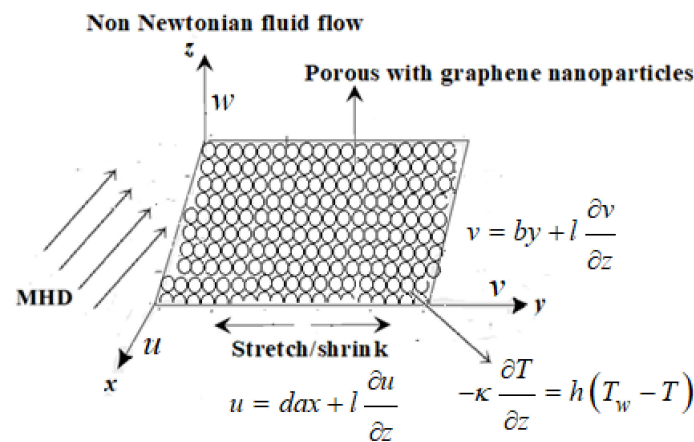

Figure 1. Physical diagram of three-dimensional fluid flow.

Table 1. Thermophysical properties of base fluid and nanoparticles.

	C_P (**J/kgK**)	ρ (**kg/m³**)	k (**W/mK**)	σ $(\Omega/\text{m})^{-1}$
Pure water (H₂O)	4179	997.1	0.613	0.05
Graphene (G)	2100	2250	2500	1×10^7

The heat flux q_r can be defined on the basis of Rosseland's approximation as follows (see refs. [35–39]):

$$q_r = -\frac{4\sigma^*}{3k^*}\frac{\partial T^4}{\partial y} \tag{6}$$

here, σ^* is the Stefan–Boltzmann constant, k^* is the coefficient of mean absorption, and T is the temperature of the fluid.

Ambient temperature T^4 expands in terms of Taylor's series as

$$T^4 = T_\infty^4 + 4T_\infty^3(T - T_\infty) + 6T_\infty^2(T - T_\infty)^2 + \ldots \tag{7}$$

In Equation (7), we ignore higher order terms to yield the equation as

$$T^4 = -3T_\infty^4 + 4T_\infty^3 T \tag{8}$$

On applying Equation (8) into Equation (6), the first order derivative of heat flux can be given by

$$\frac{\partial q_r}{\partial y} = -\frac{16\sigma^* T_\infty^3}{3k^*}\frac{\partial^2 T}{\partial y^2} \tag{9}$$

the physical quantities used in Equations (1) to (9) are defined in the Nomenclature.

Now, the subsequent similarity transformations utilized can be defined as

$$\left.\begin{array}{ll} \eta = \sqrt{\frac{a}{\nu}}z, & u = axf_\eta(\eta), & v = ayg_\eta(\eta) \\ w = -\sqrt{a\nu}(f(\eta) + g(\eta)), & \theta(\eta) = \frac{T-T_\infty}{T_w-T_\infty} \end{array}\right\} \tag{10}$$

We use these similarity transformations in Equations (1) to (4) to calculate the following ODEs

$$\frac{\varepsilon_1}{\varepsilon_2}f_{\eta\eta\eta} + f_{\eta\eta}(f+g) - f_\eta^2 + \gamma f_\eta - \left(\frac{\varepsilon_1}{\varepsilon_2}Da^{-1} + \frac{\varepsilon_3}{\varepsilon_2}M\right)f_\eta$$
$$+ \beta\{f_{\eta\eta\eta\eta}(f+g) + f_{\eta\eta}(f_{\eta\eta} - g_{\eta\eta}) - 2f_{\eta\eta\eta}(f_\eta + g_\eta)\} = 0 \tag{11}$$

$$\frac{\varepsilon_1}{\varepsilon_2}g_{\eta\eta\eta} + g_{\eta\eta}(f+g) - g_\eta^2 + \gamma g_\eta - \left(\frac{\varepsilon_1}{\varepsilon_2}Da^{-1} + \frac{\varepsilon_3}{\varepsilon_2}M\right)g_\eta$$
$$+ \beta\{g_{\eta\eta\eta\eta}(f+g) + g_{\eta\eta}(g_{\eta\eta} - f_{\eta\eta}) - 2g_{\eta\eta\eta}(f_\eta + g_\eta)\} = 0 \tag{12}$$

$$(\varepsilon_5 + R)\theta_{\eta\eta} + \mathrm{Pr}\varepsilon_4\theta_\eta(f+g) = 0 \tag{13}$$

Reduced boundary conditions are as follows,

$$\left.\begin{array}{lll} f_\eta(0) = d + Lf_{\eta\eta}(0), & f(0) = V_C, & f_\eta(\infty) \to 0, & f_{\eta\eta}(\infty) \to 0, \\ g(0) = c + Lg_{\eta\eta}(0), & g_\eta(\infty) \to 0, & & g_{\eta\eta}(\infty) \to 0, \\ \theta_\eta(0) = -Bi(1 - \theta(0)), & \theta(\infty) \to 0, & & \end{array}\right\} \tag{14}$$

Here, $Da^{-1} = \frac{\mu_f}{\rho_f Ka}$, is an inverse Darcy number, $M = \frac{\sigma_f B_0^2}{\rho_f a}$, is a Hartman number, $\beta = \frac{ka}{\nu}$ is a viscoelastic parameter, $\gamma = \frac{\gamma_0}{a}$ indicates the parameter of porosity, $L = l\sqrt{\frac{a}{\nu}}$ is the first order velocity slip parameter, $V_C = -\frac{w_0}{\sqrt{a\nu}}$ indicates mass transpiration with $V_C > 0$ denotes suction, $V_C < 0$ indicates injection, $V_C = 0$ for impermeable sheet, and $\mathrm{Pr} = \frac{(\mu C_P)_f}{\kappa_f}$ is a Prandtl number. d and $c = \frac{b}{a}$ denotes the stretching/shrinking sheet parameters along the x and y axis, respectively. If $d = 1$, it indicates stretching rate; if $d = -1$, it indicates shrinking rate.

The nanofluid quantities used in Equations (11) to (13) can be defined as (see Afridi et al. [40] and Afridi and Qasim [41]):

$$\varepsilon_1 = \frac{\mu_{nf}}{\mu_f}, \quad \varepsilon_2 = \frac{\rho_{nf}}{\rho_f}, \quad \varepsilon_3 = \frac{\sigma_{nf}}{\sigma_f}, \quad \varepsilon_4 = \frac{(\rho C_P)_{nf}}{(\rho C_P)_f}, \quad \varepsilon_5 = \frac{\kappa_{nf}}{\kappa_f} \tag{15}$$

Moreover, for our convenience, we use $\Gamma = \gamma - \left(\frac{\varepsilon_1}{\varepsilon_2}Da^{-1} + \frac{\varepsilon_3}{\varepsilon_2}M\right)$ in the further mathematical sequel, this term combines the magnetic interaction $M > 0$, porosity parameter γ, and inverse Darcy number Da^{-1}.

2. Analytical Solutions

2.1. Analytical Solution of Momentum Equation

Based on the analytical solution derived in Crane [3], Aly [42], and Mahabaleshwar et al. [43], for some special cases of stretching sheet problems, we assume the solutions of Equations (11) and (12) are of the form

$$f(\eta) = V_C + \frac{d(1 - \exp(-\lambda\eta))}{\lambda(1 + L\lambda)} \tag{16}$$

$$g(\eta) = \frac{d(1 - \exp(-\lambda\eta))}{\lambda(1 + L\lambda)} \tag{17}$$

The solutions defined in Equations (16) and (17) satisfy all the boundary conditions defined in Equation (14), then substitute these solutions into Equation (11) at the limiting value $\eta \to \infty$ to find the following resulting equations:

$$(-\varepsilon_1 + 2\beta d\varepsilon_2)\lambda^2 + 2d\varepsilon_2 = 0 \tag{18}$$

$$-2d\left(1 + \beta\lambda^2\right)\varepsilon_2 + (1 + L\lambda)\left(\gamma\varepsilon_2 - \left(\varepsilon_1 Da^{-1} + \varepsilon_3 M\right)\right) - \lambda\left(V_C - \varepsilon_1\lambda + \varepsilon_2\beta V_C\lambda^2\right) = 0 \tag{19}$$

Solving above two solutions yields the following results:

$$\lambda = \sqrt{\frac{2\varepsilon_2}{2\beta\varepsilon_2 - \varepsilon_1}}$$

$$V_C = \frac{-2d\varepsilon_2\left(1 + \beta\lambda^2\right) - (\varepsilon_1\Lambda + \varepsilon_3 M - \gamma\varepsilon_2)(1 + L\lambda) + \varepsilon_1\lambda^2(1 + L\lambda)}{\lambda(1 + \beta\lambda^2)(1 + L\lambda)} \tag{20}$$

Further, the local skin friction coefficient can be determined as

$$f_{\eta\eta}(0) = g_{\eta\eta}(0) = -\frac{\lambda d}{(1 + L\lambda)} \tag{21}$$

2.2. Analytical Solution of Energy Equation

Introducing a new variable ξ as

$$\xi = \frac{\text{Pr}}{\lambda^2} e^{-\lambda\eta}, \tag{22}$$

on substituting Equation (22) in Equation (13) to achieve the equation

$$(\varepsilon_5 + R)\xi\frac{\partial^2\theta}{\partial\xi^2} + \left\{(\varepsilon_5 + R) - \varepsilon_4\text{Pr}\left(\frac{V_C\lambda(1 + L\lambda) + 2d}{\lambda^2(1 + L\lambda)}\right) + \frac{2d\varepsilon_4}{1 + L\lambda}\xi\right\}\frac{\partial\theta}{\partial\xi} = 0 \tag{23}$$

the boundary condition reduces to

$$\frac{\text{Pr}}{\lambda}\left(\theta_\eta\left(\frac{\text{Pr}}{\lambda^2}\right)\right) = -Bi\left(1 - \theta\left(\frac{\text{Pr}}{\lambda^2}\right)\right), \; \theta(0) = 0 \tag{24}$$

After solving Equations (23) and (24), the solution of the energy equation becomes

$$\theta(\eta) = \frac{Bi\,\Gamma\left(1 - \frac{B}{C}, 0\right) - Bi\,\Gamma\left(1 - \frac{B}{C}, \frac{-2d\varepsilon_4\text{Pr}}{(1+L\lambda)\lambda^2}\exp(-\lambda\eta)\right)}{\lambda\left(\frac{-2d\varepsilon_4\text{Pr}}{(1+L\lambda)\lambda^2}\right)^{1-\frac{B}{C}}\exp\left(\frac{-2d\varepsilon_4\text{Pr}}{(1+L\lambda)\lambda^2}\right) + Bi\left\{\Gamma\left(1 - \frac{B}{C}, 0\right) - \Gamma\left(1 - \frac{B}{C}, \frac{-2d\varepsilon_4\text{Pr}}{(1+L\lambda)\lambda^2}\right)\right\}} \tag{25}$$

where,

$$B = (\varepsilon_5 + R) - \varepsilon_4\text{Pr}a$$
$$C = (\varepsilon_5 + R) \tag{26}$$
$$a = \frac{V_C\lambda(1 + L\lambda) + 2d}{\lambda^2(1 + L\lambda)}$$

3. Results and Discussions

Three-dimensional nanofluid flow due to a porous stretching/shrinking sheet with mass transpiration and radiation is examined in the current analysis. The resulting non-linear PDES are altered into ODEs with the help of similarity transformations, then the problem is verified analytically, and mass transpiration is solved under a special case. The energy equation is solved with a Biot number. Graphene nanofluid volume fraction is used to derive the problem analytically. The analytical solution of momentum and energy equation is indicated in Equations (20) and (25), respectively. In solution domain, λ can be linked through Equation (20), the mass transpiration depends on λ, Γ, β and L, and

the temperature profile depends on V_C, R, Pr, λ and d. The physical scenario can be understood with the help of different physical parameters, then by using this we conclude the following discussion.

Figure 2a,b represents the effect of transverse velocity $f(\eta)$ verses similarity variable η for different choices of Γ for stretching and shrinking cases, respectively, with fixed the parameters as $d = 1$, $\beta = \phi = 0.1$. Here, it is seen that the transverse velocity $f(\eta)$ decreases with an increase in the values of Γ. Here, the red solid lines portray the flow patterns at $L = 0$ and black solid lines portray the flow patterns at $L = 0.5$. From these figures, it seems that the boundary value thickness is wider for the shrinking sheet case compared to the stretching sheet case. Additionally, the velocity is higher for more values of L for the stretching sheet case, but this effect is reversed for the shrinking sheet case.
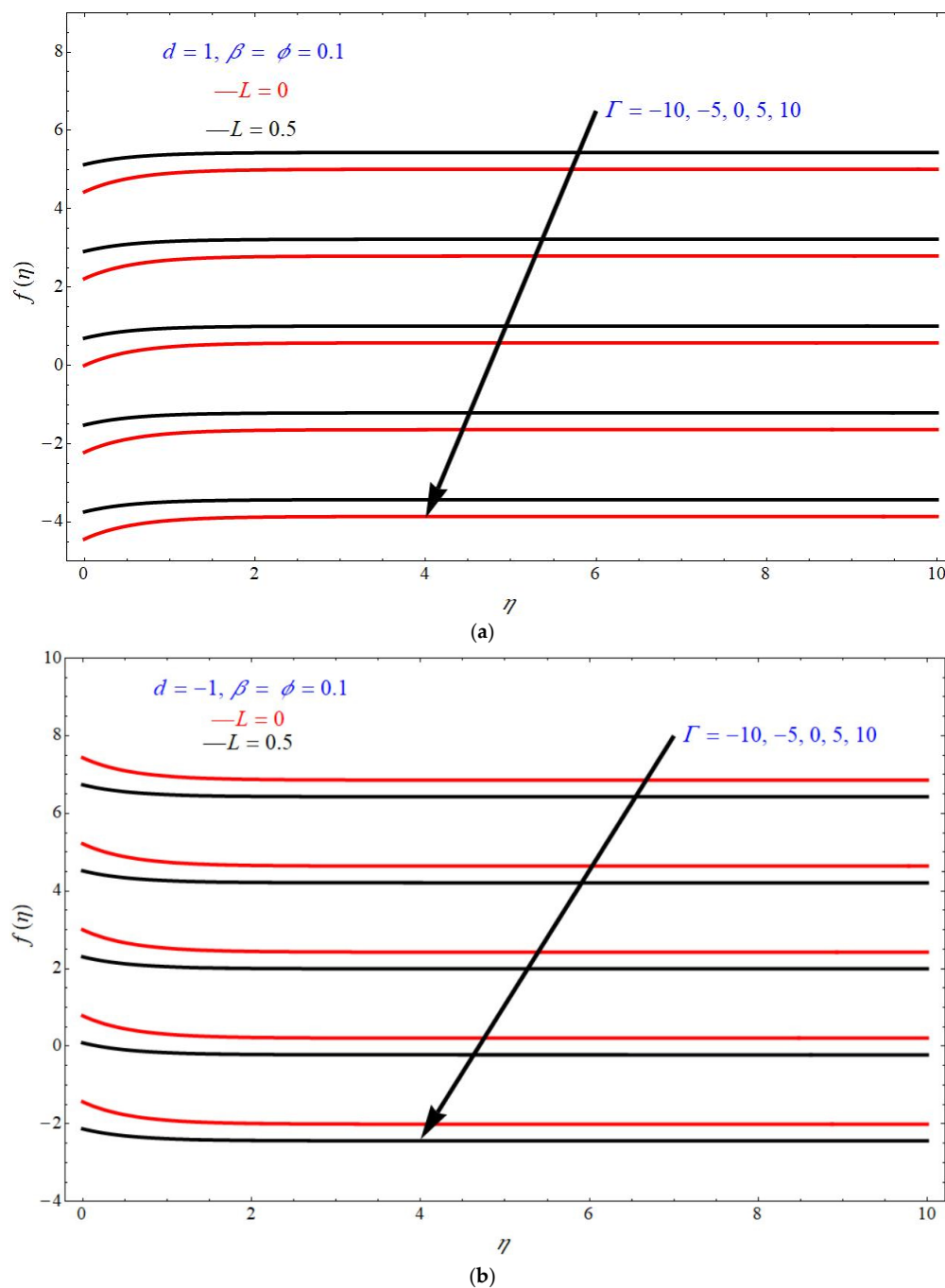

Figure 2. Effect of $f(\eta)$ on η for various choices of Γ (**a**) stretching and (**b**) shrinking cases.

Figure 3a,b represents the impact of tangential velocity $f_\eta(\eta)$ on η for various values of β and ϕ respectively, keeping the parameters $d = \Gamma = 1$, $\phi = 0.1$ at Figure 3a and $d = \Gamma = 1$, $\beta = 0.1$ at Figure 3b. From these figures, we can conclude that the tangential velocity $f_\eta(\eta)$ increases with increase in the values of β and ϕ. Here, the red solid lines also represent the flow patterns at $L = 0$ and the black solid lines portray the flow patterns at $L = 0.5$. Here, the unknown λ value linked with these parameters through Equation (20). Physically, the parameter Γ is the combination of a magnetic interaction, inverse Darcy number, and porosity parameter. Mathematically, it is represented as follows

$$\Gamma = \gamma - \left(\frac{\varepsilon_1}{\varepsilon_2} Da^{-1} + \frac{\varepsilon_3}{\varepsilon_2} M \right) \tag{27}$$

This parameter controls the domain of existence and permits the presence of solutions for both wall transpirations for $\Gamma < 0$, whereas mass suction corresponds to the certain values of $\Gamma \geq 0$. It is also observed that existence domain seems to be wider for the stretching sheet case as compared to the shrinking sheet case. Increasing slip or increasing viscoelasticity decreases the shear stress. In these figures, the impact of Γ helps to control the uniformity of the flow and to calculate the values of η.
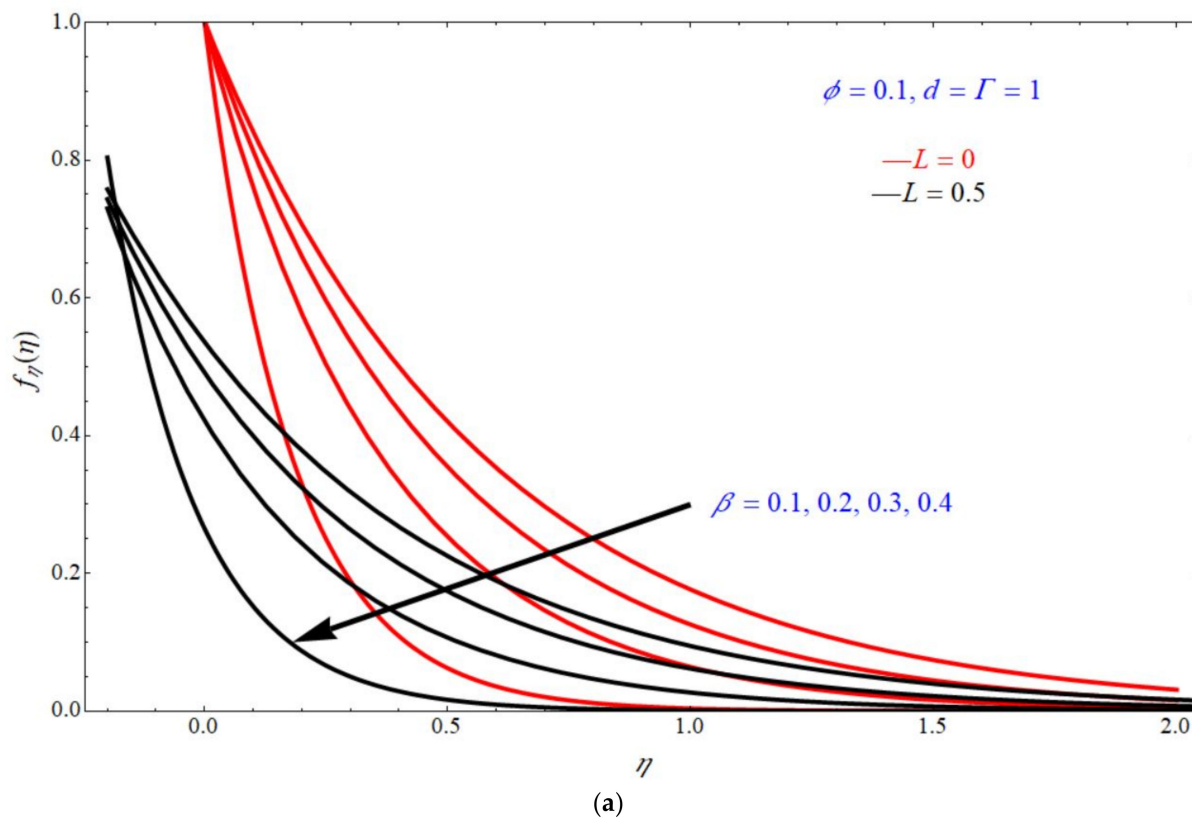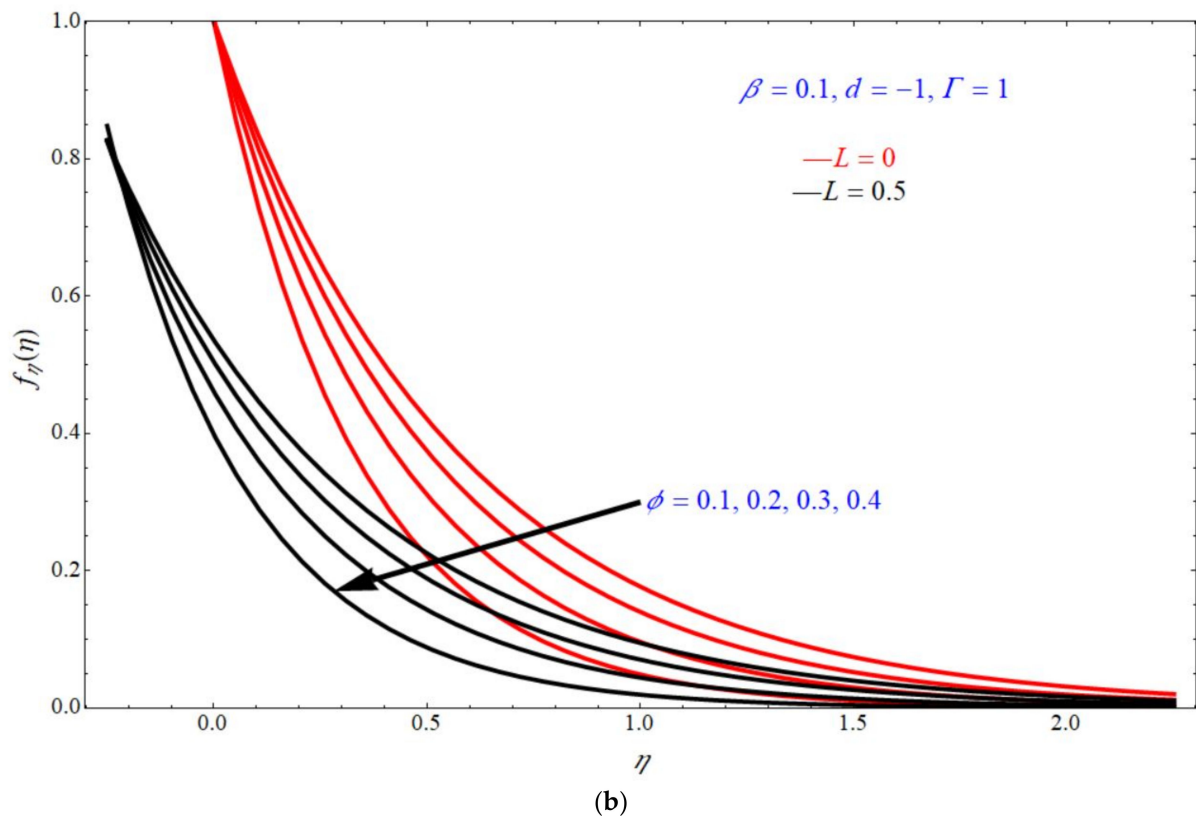

(a)

Figure 3. *Cont.*

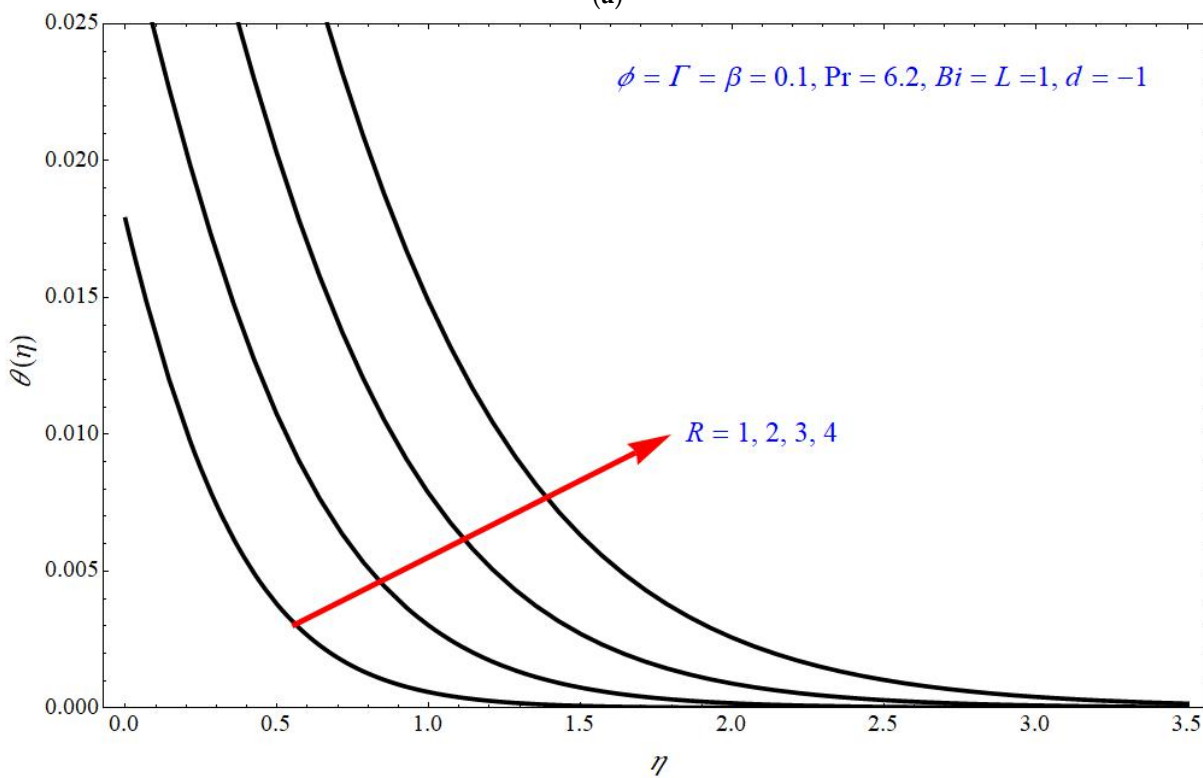**Figure 3.** Impact of $f_\eta(\eta)$ on η for various choices of (**a**) β and (**b**) ϕ.

Equation (25) depicts the analytical expression of the energy equation along with a Biot number; this expression can provide the analytical solution of the temperature for Γ, R, ϕ & β; the thermal analysis is valid for $\text{Pr} = 6.2$, $\beta < 1$, $\phi < 1$ and the slip parameter is fixed to $L = 1$. According to the laminar boundary layer theory, the dependence of all these numbers and parameters are discussed below. Figures 4–7 depict the impact of temperature profile $\theta(\eta)$ verses similarity variable η for different choices of different physical parameters. Figure 4a,b depict the impact of $\theta(\eta)$ verses η for various values of Γ at $d = 1$ and $d = -1$, respectively, with the fixed parameters $\phi = \beta = 0.1$, $R = Bi = 1$. In both the stretching and shrinking cases, the $\theta(\eta)$ increases with an increase in the values of Γ. $\theta(\eta)$ increases with increases in the values of R for both $d = 1$ and $d = -1$ indicated, respectively, in Figure 5a,b. In this case, the other parameters are fixed to $\phi = \Gamma = \beta = 0.1$, $Bi = 1$. Figure 6a,b depict the impact of $\theta(\eta)$ verses η for various choices of ϕ; here, it is seen that $\theta(\eta)$ increases with increases of ϕ for both stretching and shrinking cases, and the other parameters are fixed to $\Gamma = \beta = 0.1$, $R = Bi = 1$. Figure 7a,b demonstrate the effect of temperature profile $\theta(\eta)$ verses η for various values of β, keeping the other parameters as $\phi = \Gamma = 0.1$, $R = Bi = 1$. Here, it is seen that $\theta(\eta)$ increases with an increase in the values of β for both $d = 1$ and $d = -1$.
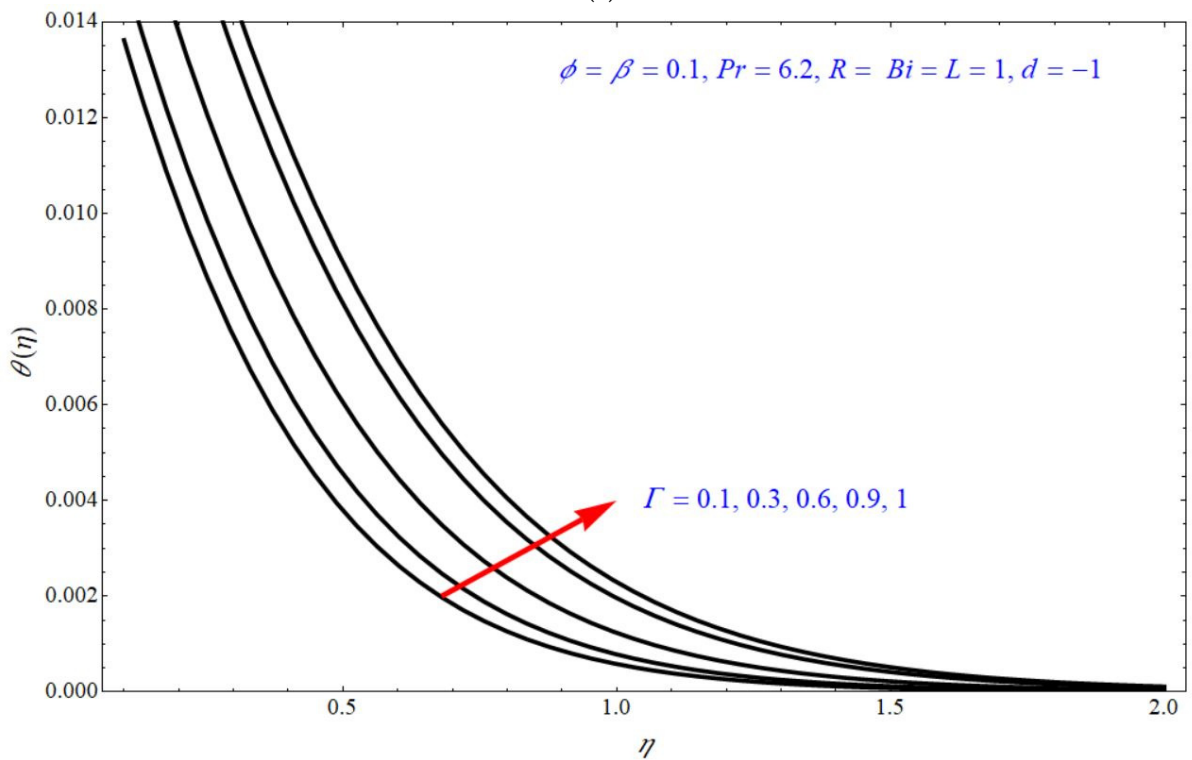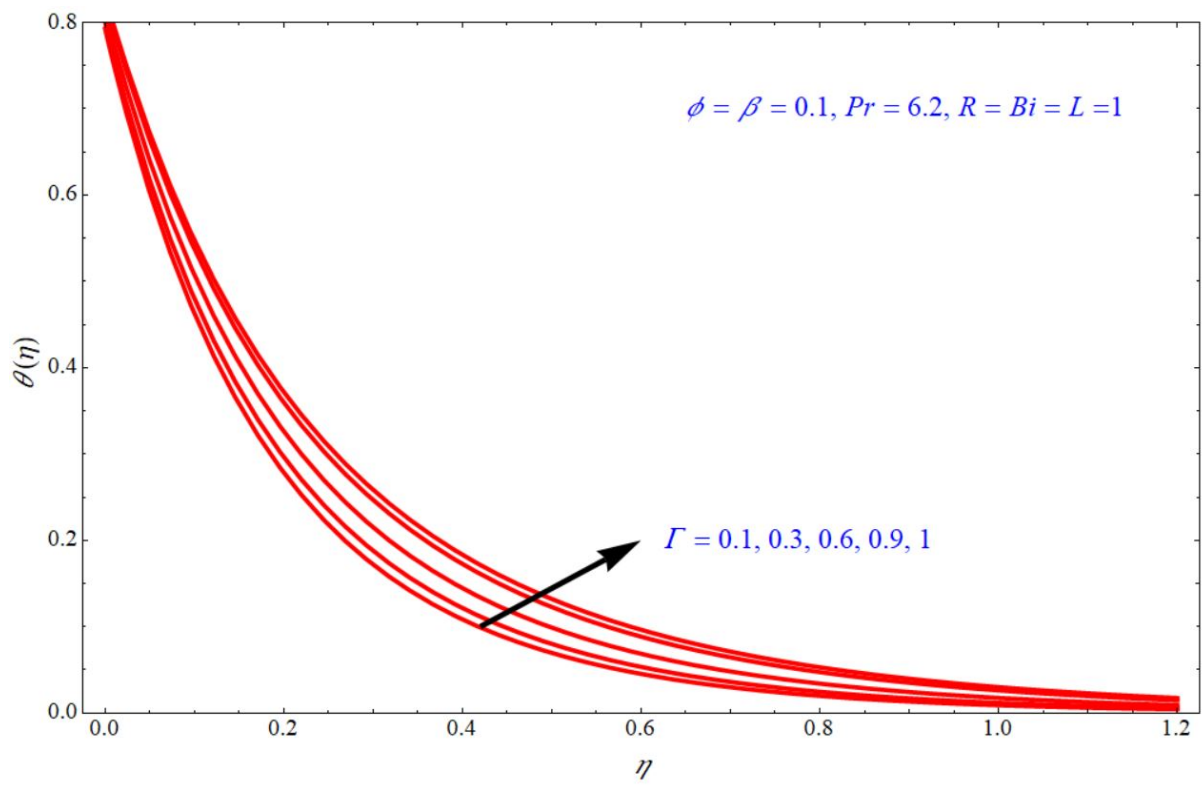
Figure 4. Impact of $\theta(\eta)$ on η for different choices of Γ at (**a**) $d = 1$ and (**b**) $d = -1$.
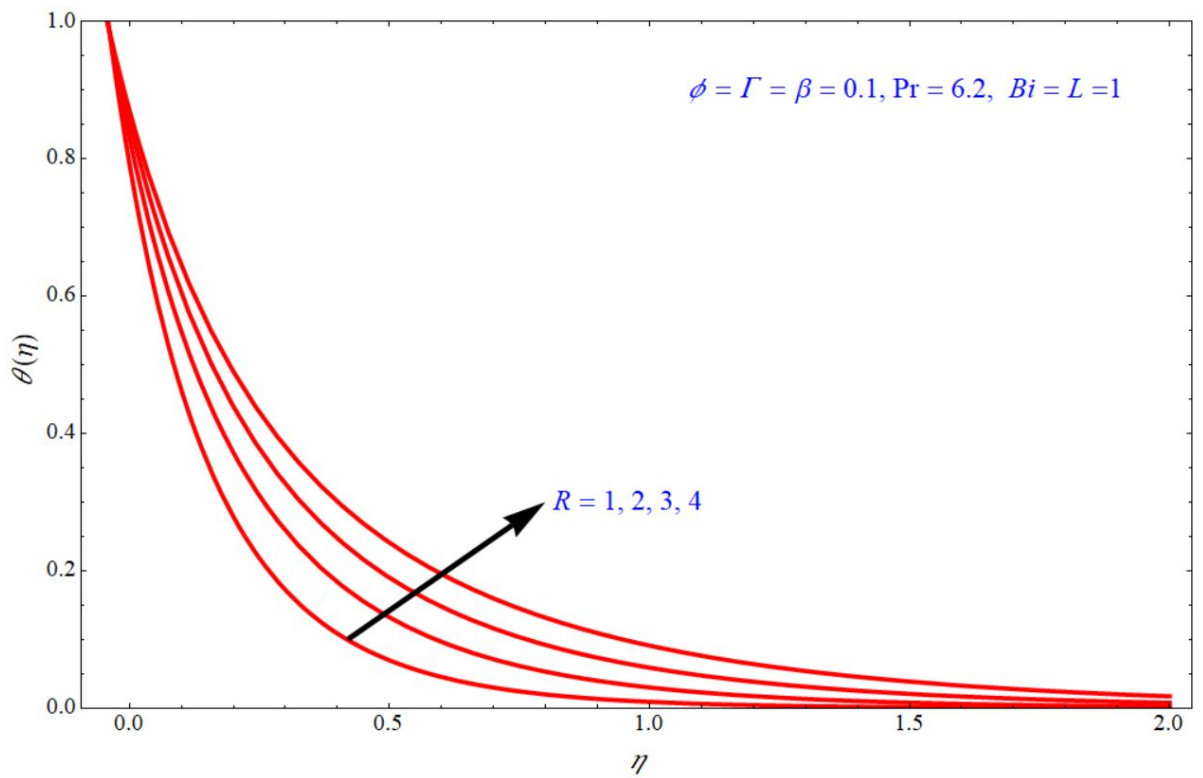
Figure 5. Impact of $\theta(\eta)$ on η for various choices of R at (**a**) $d = 1$ and (**b**) $d = -1$.

Pr = 6.2, $\beta = \Gamma = 0.1$, $R = Bi = L = 1$

$\phi = 0.1, 0.125, 0.15, 0.175, 0.2$

(**a**)

Pr = 6.2, $\beta = \Gamma = 0.1$, $R = Bi = L = 1$
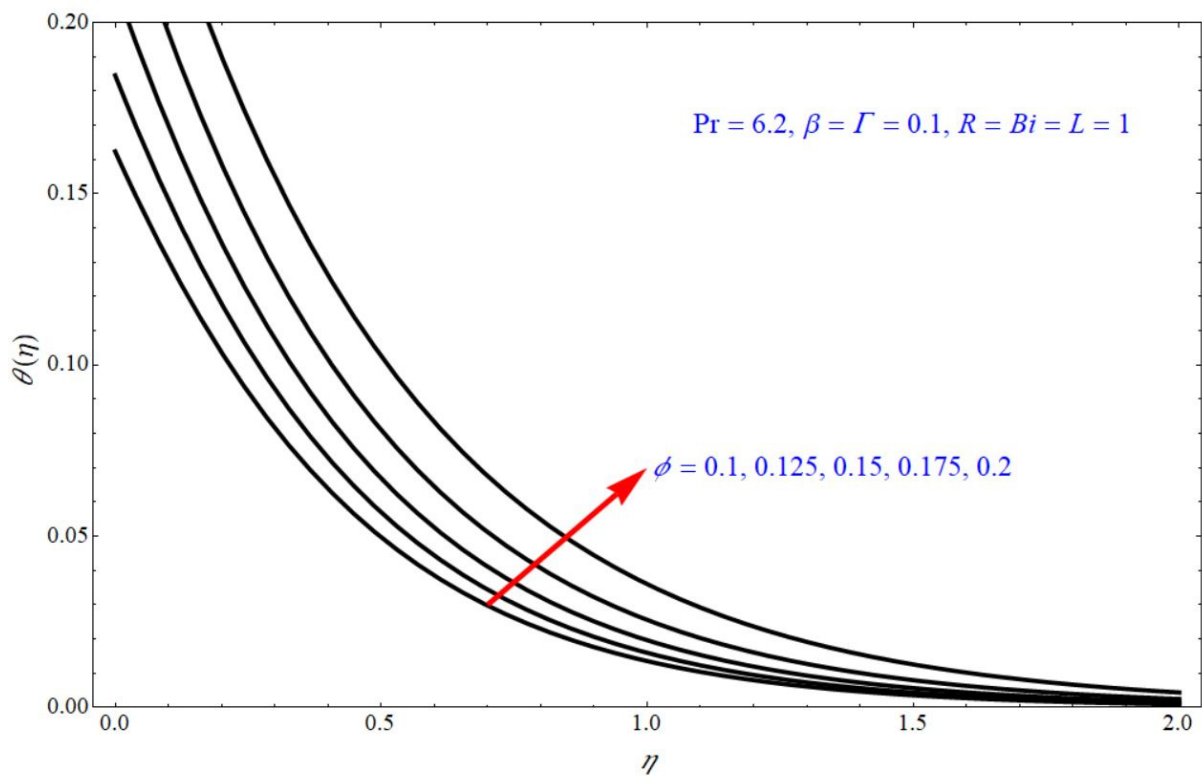
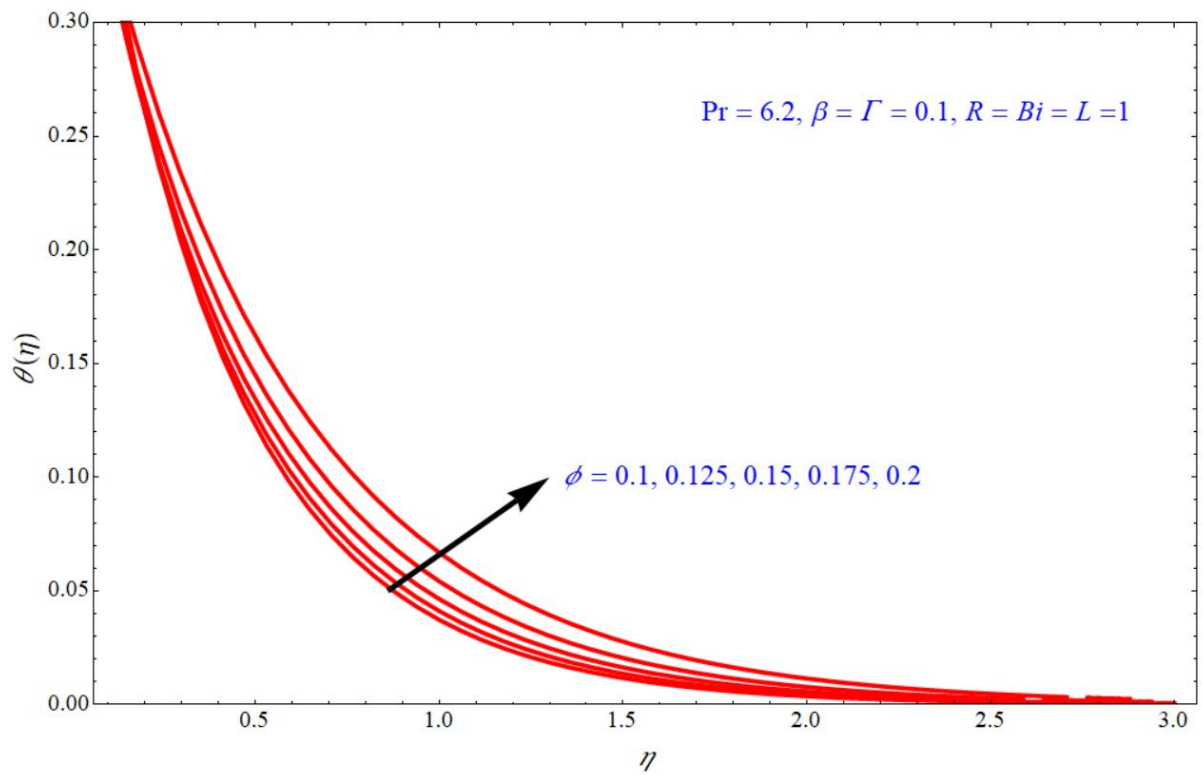$\phi = 0.1, 0.125, 0.15, 0.175, 0.2$

(**b**)

Figure 6. Impact of $\theta(\eta)$ on η for various choices of ϕ at (**a**) $d = 1$ and (**b**) $d = -1$.

(**a**)

(**b**)
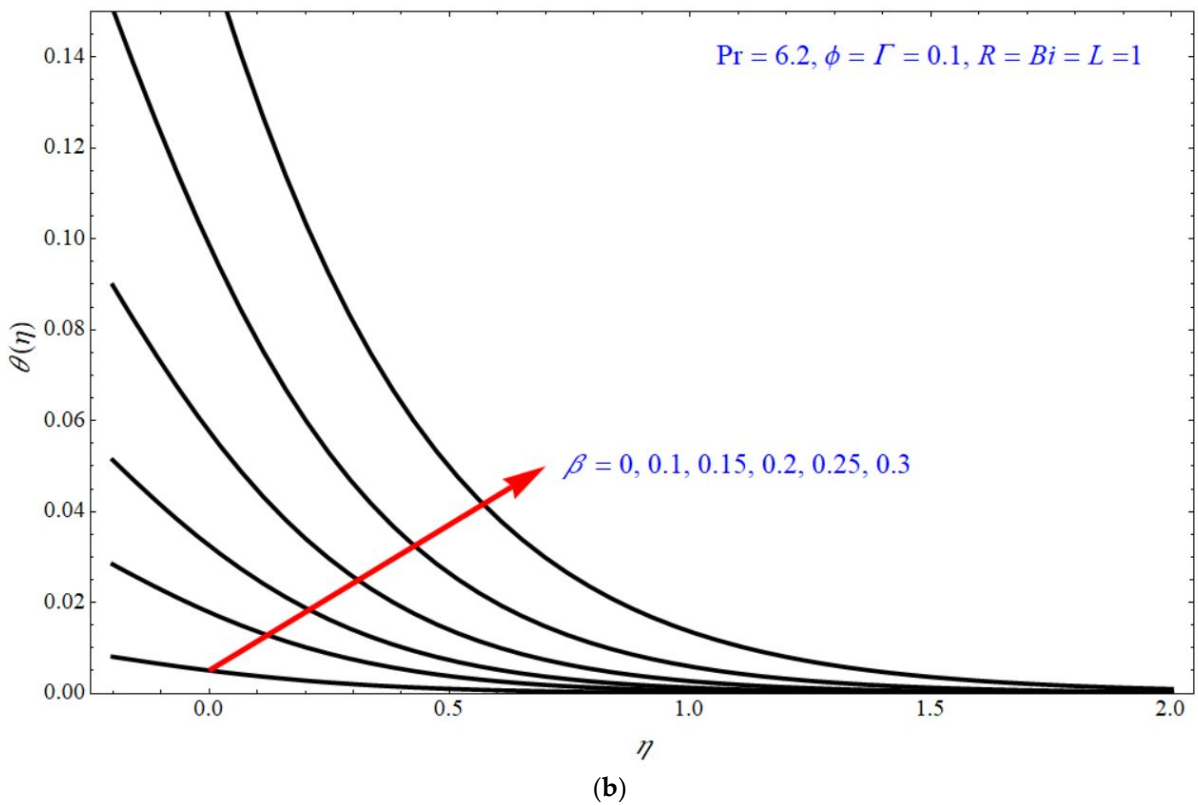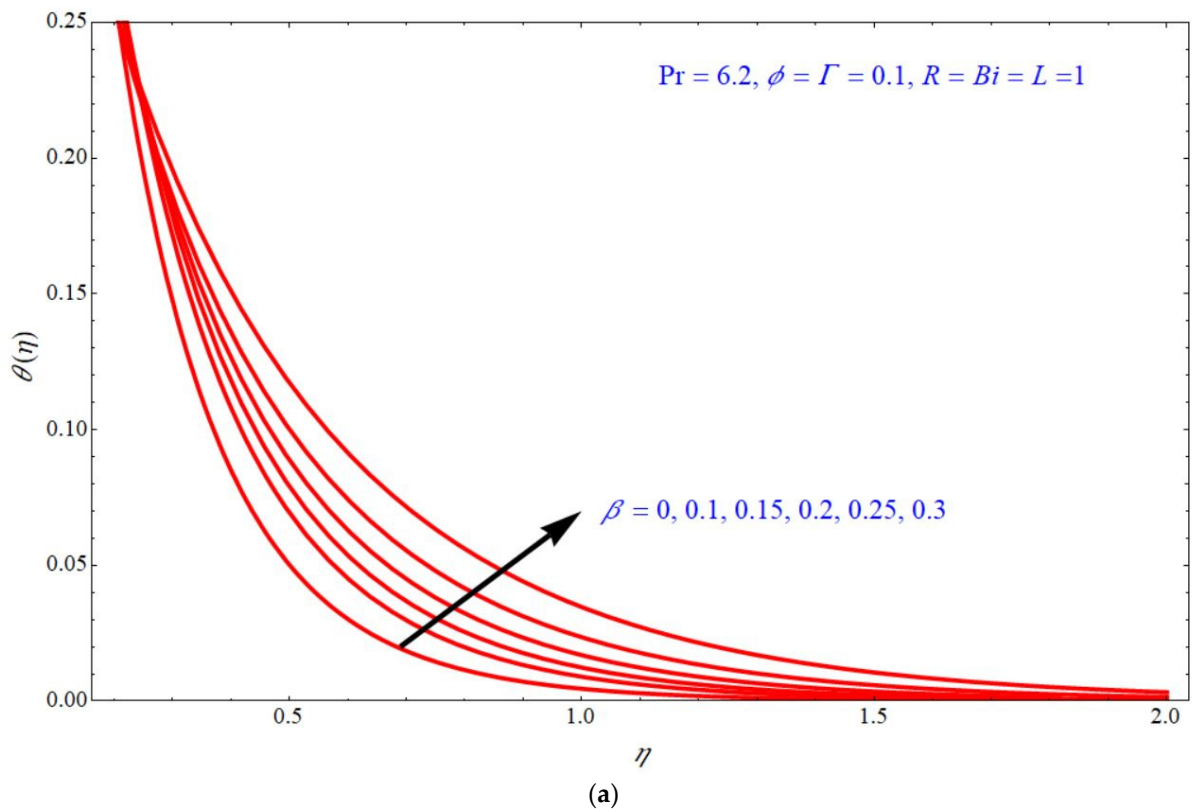
Figure 7. Impact of $\theta(\eta)$ on η for various choices of β at (**a**) $d = 1$ and (**b**) $d = -1$.

Figure 8a,b depict the impact of mass transpiration V_C on solid volume fraction ϕ for various values of Γ. Domain V_C moves towards negative values if we increase the values of Γ for both stretching and shrinking cases. Here, it seems to be that the shrinking case is wider than the stretching case.
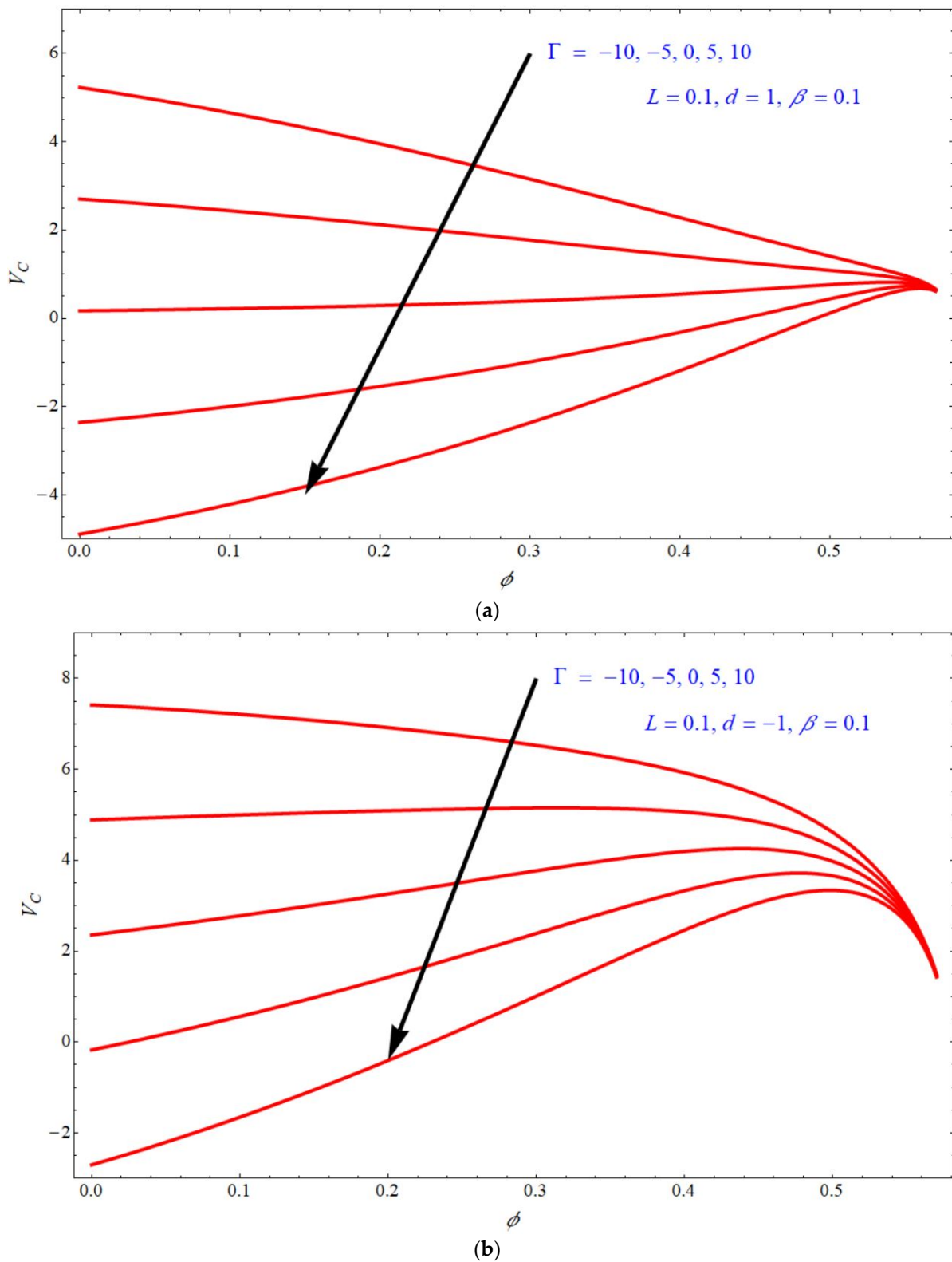
Figure 8. Impact of V_c on ϕ for various choices of Γ at (**a**) $d = 1$ and (**b**) $d = -1$.

The incomplete gamma function $\Gamma(a, z)$ becomes infinite when $a = z = 0$. This knowledge is very significant for gaining the knowledge about Nusselt number and threshold parameters. This leads to the first non-zero heat transfer rate which is triggered by the incomplete gamma function; these results are not discussed much in our work (see Turkyilmazoglu [28]).

4. Concluding Remarks

An investigation has taken place on 3-D MHD graphene water nanofluid through porous media in the presence of mass transpiration and radiation. A closed form solution is obtained for both the flow and temperature, and mass transpiration is solved under a special case. Slip condition was also taken into account. The present work is useful in many real-life applications such automotive cooling systems, power generation, microelectronics, and air conditioning.

By using this analysis, the following results can be concluded:

- Stretching case is wider than shrinking case.
- Velocity decreases with increases in the values of Γ.
- Tangential velocity $f_\eta(\eta)$ decreases with an increase in the values of β and ϕ.
- $\theta(\eta)$ is more for more values of Γ and R for both the stretching and shrinking cases.
- $\theta(\eta)$ is increases with increases in the values of ϕ and β in the stretching case and the shrinking case.
- The limiting parameters $Da^{-1} = \phi = R = 0$, ε_1 to $\varepsilon_5 = 1$, $Bi \to \infty$. in the present work is transformed into the work of Turkyilmazoglu [28] work.
- The classical Crane (1970) flow is recovered if the limiting parameters $M = \beta = Da^{-1}$ $= \phi = R = L = \gamma = 0$, ε_1 to $\varepsilon_5 = 1$, $Bi \to \infty$.

Author Contributions: U.S.M. and A.B.V. conceptualized, modelled, and solved the problem, performed formal analysis, contributed to analytical computations, plotted the graphical results, wrote the original draft, and investigated the problem. And perform programming in Mathematica. I.E.S. also contributed to modelling and solving the problem, writing, review and editing and validation of the results. All authors finalized the manuscript after its internal evaluation. All authors have read and agreed to the published version of the manuscript.

Data Availability Statement: Data sharing is not applicable to this article.

Conflicts of Interest: The author declare no conflict of interest.

Nomenclature

List of variables	Description	S.I. Units
a	Constants	(s^{-1})
B_0	Strength of uniform magnetic field	(Tesla)
Bi	Biot number	$(-)$
b	Constant	(s^{-1})
C_P	Specific heat at constant Pressure	$(Jkg^{-1}K^{-1})$
$d \& c$	Stretching/shrinking parameter along x and y axis	$(-)$
Da^{-1}	Inverse Darcy number	$(-)$
f	Non dimensional transverse velocity	$(-)$
g	Non dimensional velocity	$(-)$
f_η	Non dimensional Tangential velocity	$(-)$
k	Material constant	(W/mK)
h	Heat transfer coefficient	$(-)$
k	Material constant	(W/mK)
k^*	Coefficient of mean absorption	(m^{-2})
K	Permeability of porous medium	(m^2)
L	Coefficient of first order slip	$(-)$
l	Characteristic length	$(-)$
M	Hartman number	$(-)$
Pr	Prandtl number	$(-)$
q_r	Radiative heat flux	$(-)$
q_w	Local heat flux	(Wm^{-2})

R	Radiation parameter	$(-)$
V_c	Mass transpiration	$(-)$
T_∞	Far field temperature	(K)
T_w	Wall temperature	(K)
T	Temperature	(K)
(u, v, w)	Velocities along x, y, and z direction, respectively	(ms^{-1})
(x, y, z)	Cartesian coordinates	(m)
w_0	Wall transpiration	(ms^{-1})
Greek symbols		
β	Dimensionless viscoelastic parameter	$(-)$
λ	Solution domain	$(-)$
η	Similarity variable	$(-)$
γ	Porosity parameter	$(-)$
γ_0	Porosity	$(-)$
μ	Dynamic viscosity	$(\mathrm{m}^{-1}\mathrm{s}^{-1})$
ν	Kinematic viscosity	$(\mathrm{m}^2\mathrm{s}^{-1})$
κ	Thermal conductivity	$(\mathrm{Wm}^{-1}\mathrm{K}^{-1})$
ρ	Fluid density	(kgm^{-3})
θ	Dimensionless temperature	$(-)$
σ	Electric conductivity	(Sm^{-1})
σ^*	Stefan–Boltzmann constant	$(\mathrm{Wm}^{-2}\mathrm{K}^{-4})$
$\Gamma(a, z)$	Incomplete gamma function	$(-)$
Γ	Special constant used in the problem	$(-)$
Subscripts		
w	Wall condition	$(-)$
∞	Free stream condition	$(-)$
η	Differentiation with respect to η	$(-)$
Abbreviations		
MHD	Magneto hydrodynamics	$(-)$
ODEs	Ordinary differential equations	$(-)$
PDEs	Partial differential equations	$(-)$

References

1. Sakiadis, B.C. Boundary-layer behavior on continuous solid surfaces: I. Boundary-layer equations for two-dimensional and axisymmetric flow. *AIChE J.* **1961**, *7*, 26–28. [CrossRef]
2. Sakiadis, B.C. Boundary-layer behavior on continuous solid surfaces: II. The boundary layer on a continuous flat surface. *AIChE J.* **1961**, *7*, 221–225. [CrossRef]
3. Crane, L.J. Flow past a stretching plate. *Z. Angew. Math. Phys.* **1970**, *21*, 645–647. [CrossRef]
4. Turkyilmazoglu, M. Analytic heat and mass transfer of the mixed hydrodynamic/thermal slip MHD viscous flow over astretching sheet. *Int. J. Mech. Sci.* **2011**, *53*, 886–896. [CrossRef]
5. Mahabaleshwar, U.S.; Sarris, I.E.; Hill, A.A.; Lorenzini, G.; Pop, I. An MHD couple stress fluid due to a perforated sheet undergoing linear stretching with heat transfer. *Int. J. Heat Mass Transf.* **2016**, *105*, 157–167. [CrossRef]
6. Mahabaleshwar, U.S.; Nagaraju, K.R.; Kumar, P.N.V.; Nadagouda, M.N.; Bennacer, R.; Sheremet, M.A. Effects of Dufour and Sort mechanisms on MHD mixed convective-radiative non-Newtonian liquid flow and heat transfer over a porous sheet. *Therm. Sci. Eng. Prog.* **2020**, *16*, 100459. [CrossRef]
7. Mahabaleshwar, U.; Nagaraju, K.; Kumar, P.V.; Nadagoud, M.; Bennacer, R.; Baleanu, D. An MHD viscous liquid stagnation point flow and heat transfer with thermal radiation and transpiration. *Therm. Sci. Eng. Prog.* **2020**, *16*, 100379. [CrossRef]
8. Elbashbeshy, E.M.A.; Bazid, M.A. Heat transfer over a continuously moving plate embedded in a non-darcian porous medium. *Int. J. Heat Mass Transf.* **2000**, *43*, 3087–3092. [CrossRef]
9. Elbashbeshy, E.; Bazid, M. Heat Transfer Over an unsteady Stretching Surface With Internal Heat Generation. *Appl. Math. Comput.* **2003**, *138*, 239–245. [CrossRef]
10. Cortell, R. Flow and heat transfer of a fluid through a porous medium over a stretching surface with internal heat generation/absorption and suction/blowing. *Fluid Dyn. Res.* **2005**, *37*, 231–245. [CrossRef]
11. Mahabaleshwar, U.S.; Lorenzini, G. Combined effect of heat source/sink and stress work on MHD Newtonian fluid flow over a stretching porous sheet. *Int. J. Heat Technol.* **2017**, *35*, 330–335. [CrossRef]
12. Mahabaleshwar, U.S.; Sarris, I.E.; Lorenzini, G. Effect of radiation and Navier slip boundary of Walters' liquid B flow over a stretching sheet in a porous media. *Int. J. Heat Mass Transf.* **2018**, *127*, 1327–1337. [CrossRef]

13. Mahabaleshwar, U.S.; Nagaraju, K.N.; Kumar, P.N.V.; Azese, M.N. Effect of radiation on thermosolutal Marangoni convection in a porous medium with chemical reaction and heat source/sink. *Phys. Fluids* **2020**, *32*, 113602. [CrossRef]
14. Mahabaleshwar, U.S.; Kumar, P.N.V.; Nagaraju, K.R.; Bognár, G.; Nayakar, S.N.R. A New Exact Solution for the Flow of a Fluid through Porous Media for a Variety of Boundary Conditions. *Fluids* **2019**, *4*, 125. [CrossRef]
15. Rasool, G.; Shafiq, A.; Chu, Y.-M.; Bhutta, M.S.; Ali, A. Optimal Homotopic Exploration of features of Cattaneo-Christov model in Second Grade Nanofluid flow via Darcy-Forchheimer medium subject to Viscous Dissipation and Thermal Radiation. *Comb. Chem. High Throughput Screen.* **2021**, *24*, 1. [CrossRef]
16. Manjunatha, S.; Puneeth, V.; Anandika, R.; Gireesha, B.J. Analysis of multilayer convective flow of a hybrid nanofluid in porous medium sandwiched between the layers of nanofluid. *Heat Transf.* **2021**, *50*, 8598–8616. [CrossRef]
17. Farooq, U.; Waqas, H.; Muhammad, T.; Khan, S.A. Heat transfer enhancement of hybrid nanofluids over porous cone. *Int. J. Chem. React. Eng.* **2021**. [CrossRef]
18. Ahmed, Z.U.; Raihan, R.; Ghaffari, O.; Ikhlaq, M. Thermal and Hydraulic Performances of Porous Microchannel Heat Sink using Nanofluids. *J. Therm. Sci. Eng. Appl.* **2021**, 1–32. [CrossRef]
19. Rahman, M.M.; Rosca, A.V.; Pop, I. Boundary layer flow of a nanofluid past a permeable exponentially shrinking/stretching surface with second order slip using Buongiorno's model. *Int. J. Heat Mass Transf.* **2014**, *77*, 1133–1143. [CrossRef]
20. Mahabaleshwar, U.S.; Kumar, P.N.V.; Sheremet, M.S. Magnetohydrodynamics flow of a nanofluid driven by a stretching/shrinking sheet with suction. *SpringerPlus* **2016**, *5*, 1907. [CrossRef]
21. Benos, L.T.; Polychronopoulos, N.D.; Mahabaleshwar, U.S.; Lorenzini, G.; Sarris, I.E. Thermal and flow investigation of MHD natural convection in a nanofluid-saturated porous enclosure: An asymptotic analysis. *J. Therm. Anal.* **2021**, *143*, 751–765. [CrossRef]
22. Shafiq, A.; Rasool, G.; Alotaibi, H.; Aljohani, H.; Wakif, A.; Khan, I.; Akram, S. Thermally Enhanced Darcy-Forchheimer Casson-Water/Glycerine Rotating Nanofluid Flow with Uniform Magnetic Field. *Micromachines* **2021**, *12*, 605. [CrossRef] [PubMed]
23. Rasool, G.; Shafiq, A.; Alqarni, M.; Wakif, A.; Khan, I.; Bhutta, M. Numerical Scrutinization of Darcy-Forchheimer Relation in Convective Magnetohydrodynamic Nanofluid Flow Bounded by Nonlinear Stretching Surface in the Perspective of Heat and Mass Transfer. *Micromachines* **2021**, *12*, 374. [CrossRef] [PubMed]
24. Rasool, G.; Shafiq, A. Numerical exploration of the features of thermally enhanced chemically reactive radiative Powell-Eyring nanofluid flow via Darcy medium over non-linearly stretching surface affected by a transverse magnetic field and convective boundary conditions. *Appl. Nanosci.* **2020**. [CrossRef]
25. Afridi, M.I.; Qasim, M.; Saleem, S. Second Law Analysis of Three Dimensional Dissipative Flow of Hybrid Nanofluid. *J. Nanofluids* **2018**, *7*, 1272–1280. [CrossRef]
26. Lu, D.; Afridi, M.; Allauddin, U.; Farooq, U.; Qasim, M. Entropy Generation in a Dissipative Nanofluid Flow under the Influence of Magnetic Dissipation and Transpiration. *Energies* **2020**, *13*, 5506. [CrossRef]
27. Das, S.; Giri, A.; Samanta, S.; Kanagaraj, S. Role of graphene nanofluids on heat transfer enhancement in thermopyphon. *J. Sci. Adv. Mater. Devices* **2019**, *4*, 163–169. [CrossRef]
28. Divya, P.; Bhanvase, A.; Sonawane, H. A Review on Graphene Derivatives-based nanofluids: Investigation on properties and heat transfer characteristics. *Ind. Eng. Chem. Res.* **2020**, *59*, 10231–10277.
29. Singh, S.; Verma, P.; Ghosh, S.K. Numerical and experimental analysis of performance in a compact plate heat exchanger using graphene oxide/water nanofluid. *Int. J. Numer. Methods Heat Fluid Flow* **2021**, *31*, 3356–3372. [CrossRef]
30. Turkyilmazoglu, M. Three dimensional MHD flow and heat transfer over a stretching/shrinking surface in a viscoelastic fluid with various physical effects. *Int. J. Heat Mass Transf.* **2014**, *78*, 150–155. [CrossRef]
31. Afridi, M.I.; Qasim, M. Entropy Generation in Three Dimensional Flow of Dissipative Fluid. *Int. J. Appl. Comput. Math.* **2018**, *4*, 16. [CrossRef]
32. Mahabaleshwar, U.S. Stretching Sheet and Convective Instability Problems in Newtonian, Micropolar and Viscoelastic Liquids. Ph.D. Thesis, Bangalore University, Karnataka, India, 2005.
33. Siddheshwar, P.G.; Mahabaleshwar, U.S.; Chan, A. MHD Flow of Walters' Liquid B over A Nonlinearly Stretching Sheet. *Int. J. Appl. Mech. Eng.* **2015**, *20*, 589–603. [CrossRef]
34. Riaz, N.; Qasim, M.; Afridi, M.I.; Hussanan, A. Analysis of three-dimensional stagnation point flow over a radiation surface. *Int. Commun. Heat Mass Transf.* **2021**, *127*, 105538. [CrossRef]
35. Anusha, T.; Huang, H.-N.; Mahabaleshwar, U.S. Two dimensional unsteady stagnation point flow of Casson hybrid nanofluid over a permeable flat surface and heat transfer analysis with radiation. *J. Taiwan Inst. Chem. Eng.* **2021**, *127*, 79–91. [CrossRef]
36. Mahabaleshwar, U.S.; Anusha, T.; Sakanaka, P.H.; Bhattacharyya, S. Impact of Inclined Lorentz force and Schmidt Number on Chemically Reactive Newtonian Fluid Flow on a Stretchable Surface when Stefan Blowing and Thermal Radiation and Significant. *Arab. J. Sci. Eng.* **2021**, *46*, 12427–12443. [CrossRef]
37. Mahabaleshwar, U.S.; Sneha, K.; Huang, H.-N. An effect of MHD and radiation on CNTS-Water based nanofluids due to a stretching sheet in a Newtonian fluid. *Case Stud. Therm. Eng.* **2021**, *28*, 101462. [CrossRef]
38. Xenos, M.A.; Petropoulou, E.N.; Siokis, A.; Mahabaleshwar, U.S. Solving the Nonlinear Boundary Layer Flow Equations with Pressure Gradient and Radiation. *Symmetry* **2020**, *12*, 710. [CrossRef]
39. Aslani, K.E.; Mahabaleshwar, U.S.; Jitender, S.; Sarris, I.E. Combined effect of radiation and inclined MHD flow of a micropolar fluid over a porous stretching/shrinking sheet with mass transpiration. *Int. J. Appl. Comput. Math.* **2021**, *7*, 60. [CrossRef]

40. Afridi, M.I.; Qasim, M.; Shafie, S.; Makinde, O.D. Entropy Generation Analysis of Spherical and Non-Spherical Ag-Water Nanofluids in a Porous Medium with Magnetic and Porous Dissipation. *J. Nanofluids* **2018**, *7*, 951–960. [CrossRef]

41. Afridi, M.I.; Qasim, M. Comparitive study and entropy generation analysis of Cu-H_2O and Ag-H_2O nanofluids flow over a slandering stretching surface. *J. Nanofluids* **2018**, *4*, 783–790. [CrossRef]

42. Aly, E.H. Dual exact solutions of graphene–water nanofluid flow over stretching/shrinking sheet with suction/injection and heat source/sink: Critical values and regions with stability. *Powder Technol.* **2019**, *342*, 528–544. [CrossRef]

43. Mahabaleshwar, U.S.; Anusha, T.; Hatami, M. The MHD Newtonian hybrid nanofluid flow and mass transfer analysis due to super-linear stretching sheet embedded in porous medium. *Sci. Rep.* **2021**, *11*, 22518. [CrossRef] [PubMed]